Disorder-induced exciton localization and violation of optical selection rules in supramolecular nanotubes

Vlaming, S. M.; Bloemsma, E. A.; Nietiadi, M. Linggarsari; Knoester, J.

Published in:
Journal of Chemical Physics

DOI:
10.1063/1.3528993

Disorder-induced exciton localization and violation of optical selection rules in supramolecular nanotubes

S. M. Vlaming,[1,a)] E. A. Bloemsma,[1] M. Linggarsari Nietiadi,[1,2] and J. Knoester[1,b)]
[1]*Centre for Theoretical Physics and Zernike Institute for Advanced Materials, University of Groningen, Nijenborgh 4, 9747 AG Groningen, The Netherlands*
[2]*Institut Teknologi Bandung, Jalan Ganesha 10, Bandung 40132, Indonesia*

(Received 8 September 2010; accepted 30 November 2010; published online 16 March 2011)

Using numerical simulations, we study the effect of disorder on the optical properties of cylindrical aggregates of molecules with strong excitation transfer interactions. The exciton states and the energy transport properties of such molecular nanotubes attract considerable interest for application in artificial light-harvesting systems and energy transport wires. In the absence of disorder, such nanotubes exhibit two optical absorption peaks, resulting from three super-radiant exciton states, one polarized along the axis of the cylinder, the other two (degenerate) polarized perpendicular to this axis. These selection rules, imposed by the cylindrical symmetry, break down in the presence of disorder in the molecular transition energies, due to the fact that the exciton states localize and no longer wrap completely around the tube. We show that the important parameter is the ratio of the exciton localization length and the tube's circumference. When this ratio decreases, the distribution of polarization angles of the exciton states changes from a two-peak structure (at zero and ninety degrees) to a single peak determined by the orientation of individual molecules within the tube. This is also reflected in a qualitative change of the absorption spectrum. The latter agrees with recent experimental findings.
 [doi:10.1063/1.3528993]

I. INTRODUCTION

During the past decade, there has been a growing interest in molecular J-aggregates of cylindrical geometry.[1–14] Examples of molecules that in solution self-assemble into aggregates of a tubular shape are carbocyanine molecules with hydrophobic and hydrophilic side groups[2–7] and porphyrin derivatives.[8–12] Both these molecules yield aggregates with a diameter of the order of 10 nm and a length of up to microns, which explains why they are often referred to as molecular nanotubes. Their shape and size resemble natural light-harvesting systems in green sulphur bacteria,[1,13–18] while these systems also have a comparable geometry to previously studied helical polymers.[19–21] Because of this and the strong intermolecular excitation transfer interactions, these synthetic J-aggregates are considered excellent candidates for artificial light-harvesting systems.[22] This perspective motivates many of the recent studies of the optical absorption and luminescence properties of the collective exciton states in these systems, as well as the energy transport and relaxation caused by these states.[2–7,23–27]

In homogeneous cylindrical aggregates, the rotational symmetry around the axis imposes strong optical selection rules on the wave number k_2 that characterizes the exciton's Bloch wave function along a ring around the cylinder. In particular, it is easily shown that only states with $k_2 = 0$ and $k_2 = \pm 1$ may carry optical oscillator strength.[1,28] Further study shows that for long cylinders for each of these wave numbers only one exciton state dominates the absorption strength, as can readily be seen by imposing periodic boundary conditions in the axis direction.[1,29] As the sub-bands with opposite sign of k_2 are degenerate, a simple absorption spectrum with only two peaks is obtained, of which the one with $k_2 = 0$ is polarized along the cylinder axis, while the other one is polarized perpendicular to this axis. These simple selection rules yield a basic explanation for the experimentally observed absorption and linear dichroism spectra of tubular aggregates of the carbocyanine molecule 3,3′-bis(2-sulfopropyl)-5,5′,6,6′-tetrachloro-1,1′-dioctylbenzimidacarbocyanine (C8S3 for short).[6]

In reality, the cylindrical symmetry is broken to some extent; this may be due to the cylinder cross section not being perfectly round, due to defects within the molecular packing of the nanotube or due to the effect of local inhomogeneity of the solvent host. The latter gives rise to fluctuating local electric fields induced by the host molecules, which in turn lead to fluctuations in Stark shifts in the transition energies and the transition dipoles of the individual molecules within the aggregate.[30] As a consequence, in experiment disorder usually exists in either the transition frequencies or the intermolecular resonance interactions, or in both. Such disorder localizes the exciton states;[31] these localized states may have a much wider range of orientations of the transition dipole than just parallel and perpendicular to the cylinder axis. In the extreme case of disorder much larger than the intermolecular transfer interactions, the exciton state gets localized on just one molecule and the transition dipole of this state is simply given by the transition dipole of this molecule, which in general will be neither parallel nor perpendicular to the axis. Recent experimental work has

a)Present address: Department of Chemistry and Center for Excitonics, Massachusetts Institute of Technology, Cambridge, Massachusetts 02139, USA.
b)Electronic mail: j.knoester@rug.nl.

demonstrated that indeed the idealized selection rules are an oversimplified view of reality, in particular, in cylinders with a wider circumference.[32] Furthermore, it has also been demonstrated that by scanning near-field optical microscopy the polarization dependent luminescence of segments of individual nanotubes may be investigated,[7] which opens the perspective to look into the optical selection rules and the polarization of exciton states in much more detail.

The above situation motivates a detailed study of how broken cylindrical symmetry affects the selection rules. In this paper, we will do this for the case of disorder in the molecular transition energies (diagonal disorder), which is the type of disorder that is most frequently used to model the inhomogeneity in molecular aggregates.[33] Because of the large size of tubular aggregates, several recent papers have used the coherent potential approximation (CPA) to account for the effect of disorder on the spectra.[6,12] As the CPA does not allow for a proper description of localization, the breaking of the selection rules and the distribution of dipole orientations cannot be studied within this approach. Rather, investigating the nature of the localized exciton states requires numerical simulations, a technique applied in Refs. 34 and 35. A systematic study characterizing the breakdown of selection rules, was not conducted, however. We have done this by studying for various disorder strengths and cylinder radii, the localization behavior of the exciton wave functions, the angular distribution of the exciton transition dipoles, and the polarization dependent spectra. We have found that the parameter that governs the breakdown is the ratio of the exciton localization length and the cylinder circumference.

This paper is organized as follows. In Sec. II we present the structural and exciton model for the aggregate, and we give expressions for the isotropic and polarized absorption spectra. In Sec. III we introduce various quantities that we use to characterize the exciton localization and the breaking of the selection rules. Our numerical results are presented and discussed in Sec. IV, while we summarize and conclude in Sec. V.

II. FRENKEL EXCITON MODEL FOR CYLINDRICAL AGGREGATES

A. Geometry and Hamiltonian

Generally, the cylindrical structure of the aggregates can be obtained by rolling a two-dimensional lattice onto a cylindrical surface.[1] It is convenient to view this rolled lattice as a stack of rings, as shown in Fig. 1. Each cylinder consists of N_1 rings, each with N_2 monomers, where each ring is rotated with respect to its neighbor over an angle γ. The distance between the neighboring rings is h, while the rings have a radius R. The values of γ, h, R, and N_2 are determined by the underlying two-dimensional lattice structure and the chiral vector that defines how this lattice is rolled onto a cylinder.[1] Each molecule is labeled by the position vector $\vec{n} = (n_1, n_2)$, where n_1 labels the ring and n_2 the position in the ring (i.e., the helix on which it is located, see Fig. 1). The angles α and β define the orientation of the molecular transition dipole moments; β denotes the angle between the transition dipole moment and the cylinder axis, while α is the angle between the projection of the transition dipole moment on the ring plane and the tangent of the ring. For lattice structures with one molecule per unit cell, which we will restrict ourselves to, α and β are the same for all molecules. The above parameters fully define both the position and the transition dipole moment of each molecule,

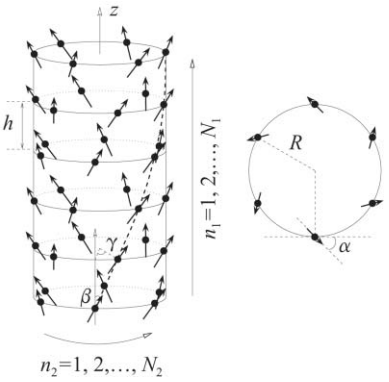

FIG. 1. The cylindrical geometry in the stack of rings representation (left) and a cross section of the cylinder perpendicular to its axis (right). The dashed helical line on the cylinder connects the molecules with $n_2 = 1$. This figure has been taken from Ref. 1.

$$\vec{r}_{\vec{n}} = (R\cos(n_2\phi_2 + n_1\gamma), R\sin(n_2\phi_2 + n_1\gamma), n_1 h), \tag{1}$$

$$\vec{\mu}_{\vec{n}} = (-\mu\sin\beta\sin(n_2\phi_2 + n_1\gamma - \alpha), \mu\sin\beta\cos(n_2\phi_2 + n_1\gamma - \alpha), \mu\cos\beta), \tag{2}$$

where μ is the magnitude of the transition dipole of an individual molecule and we have defined $\phi_2 = 2\pi/N_2$.

We use a Frenkel exciton Hamiltonian to describe the electronically excited states,[1,36,37]

$$H = \sum_{\vec{n}} \omega_{\vec{n}} b_{\vec{n}}^{\dagger} b_{\vec{n}} + {\sum_{\vec{n},\vec{m}}}' J(\vec{n} - \vec{m}) b_{\vec{m}}^{\dagger} b_{\vec{n}}, \tag{3}$$

where $\omega_{\vec{n}}$ is the excitation energy of molecule $\vec{n}$, while $b_{\vec{n}}^{\dagger}$ and $b_{\vec{n}}$ are the Pauli creation and annihilation operators for the electronic excitation of molecule $\vec{n}$. Furthermore, $J(\vec{n} - \vec{m})$ is the excitation transfer interaction between molecules $\vec{n}$ and $\vec{m}$, which depends on their (relative) positions and on their transition dipole moments. The prime on the summation excludes the term $\vec{n} = \vec{m}$. Depending on the system and the desired level of accuracy, the interactions are often taken as point dipole interactions or as extended dipole interactions. However, since the exact choice does not matter for what follows, we will keep the interactions unspecified for now. Finally, we account for disorder by taking the excitation energies $\omega_{\vec{n}}$ from a Gaussian distribution with mean ω_0 and standard deviation σ. No correlation exists between the values of $\omega_{\vec{n}}$ for different molecules. No disorder in the interactions is considered.

B. Absorption spectra

The observable quantities we are interested in are the linear absorption spectra for various polarization conditions. We assume interaction of the cylindrical aggregate with linearly

polarized light with a polarization direction $\vec{e}$ and frequency ω, and use the Fermi golden rule to account for the interaction term between light and matter. This leads to general expressions for a linear spectrum $S(\omega)$ of the form[1]

$$S(\omega) = \left\langle\left\langle \sum_q X_q \delta(\omega - E_q)\right\rangle\right\rangle, \tag{4}$$

where q labels the exciton eigenstates of the Hamiltonian Eq. (3), E_q denote the corresponding eigenenergies (we set $\hbar = 1$), and X_q are the oscillator strengths of these states for the given polarization conditions. Finally, the double angular brackets $\langle\langle ... \rangle\rangle$ denote an average over disorder realizations. The exciton eigenstates may be written as

$$|q\rangle = b_q^\dagger |g\rangle = \sum_{\vec{n}} \varphi_{q\vec{n}} b_{\vec{n}}^\dagger |g\rangle, \tag{5}$$

with $|g\rangle$ the ground state of the aggregate (all molecules in their ground state) and $\varphi_{q\vec{n}}$ the normalized coefficients of the eigenvector of the Hamiltonian corresponding to the eigenvalue E_q. Then, the (polarization dependent) oscillator strengths X_q can be written as

$$X_q = \left\langle \left| \sum_{\vec{n}} \varphi_{q\vec{n}} \vec{\mu}_{\vec{n}} \cdot \vec{e} \right|^2 \right\rangle = \sum_{\vec{n},\vec{m}} \varphi_{q\vec{n}} \varphi_{q\vec{m}}^* \langle (\vec{\mu}_{\vec{n}} \cdot \vec{e})(\vec{\mu}_{\vec{m}} \cdot \vec{e}) \rangle$$
$$\equiv \sum_{\vec{n},\vec{m}} \varphi_{q\vec{n}} \varphi_{q\vec{m}}^* X_{\vec{n}\vec{m}}, \tag{6}$$

where the single angular brackets $\langle \ldots \rangle$ denote an average over the orientation of the cylinder relative to the polarization direction $\vec{e}$.

We will consider three different polarization conditions. First of all, we will be interested in the linear absorption of an isotropic solution, $A_0(\omega)$. In this case, the cylinder orientations are distributed completely isotropically, and the spectrum does not depend on $\vec{e}$. The two other linear absorption spectra we will calculate are taken in an oriented sample, where the cylinders' axes are all aligned. This may be realized in streaming solutions, by spin coating or via microscopy experiments on single aggregates. Then, we can consider the absorption of light polarized in the cylinder axis direction $A_{||}(\omega)$ and absorption of light polarized perpendicular to the axis direction $A_\perp(\omega)$. For all three cases, it is possible to explicitly evaluate the orientational averages in Eq. (6),[1,35]

$$X_{\vec{n},\vec{m}}^0 = \tfrac{1}{3}\left(X_{\vec{n},\vec{m}}^{||} + 2X_{\vec{n},\vec{m}}^{\perp}\right),$$

$$X_{\vec{n},\vec{m}}^{||} = \mu^2 \cos^2\beta, \tag{7}$$

$$X_{\vec{n},\vec{m}}^{\perp} = \tfrac{1}{2}\mu^2 \cos\left((n_2 - m_2)\phi_2 + (n_1 - m_1)\gamma\right) \sin^2\beta.$$

The factor of 2 before the perpendicular component in the isotropic absorption strength results from the fact that there are two mutually orthogonal perpendicular directions contributing to it.

C. Selection rules in the absence of disorder

To derive the optical selection rules, we consider the homogeneous cylinder, i.e., $\omega_{\vec{n}} = \omega_0$ for all molecules $\vec{n}$. In this case, we can explicitly use the cylindrical symmetry in the ring direction and impose a Bloch form for the wave function in that direction,[1]

$$c_{n_1,k_2}^\dagger = \frac{1}{\sqrt{N_2}} \sum_{n_2} e^{ik_2\phi_2 n_2} b_{\vec{n}}^\dagger, \tag{8}$$

where k_2 is the transverse wave number that labels the Bloch state ($k_2 = 0, \pm 1, \ldots, \pm(N_2/2 - 1), N_2/2$ for N_2 even, and $k_2 = 0, \pm 1, \ldots, \pm(N_2 - 1)/2$ for N_2 odd). Using this transformation, the two-dimensional Hamiltonian Eq. (3) decouples into a set of one-dimensional Hamiltonians,[1]

$$H = \sum_{k_2} H(k_2)$$
$$= \sum_{k_2} \left(\omega_0 \sum_{n_1} c_{n_1,k_2}^\dagger c_{n_1,k_2} + \sum_{n_1,m_1} J(n_1 - m_1; k_2) c_{n_1,k_2}^\dagger c_{m_1,k_2} \right), \tag{9}$$

where the effective interaction between rings separated by $n_1 h$ is given by

$$J(n_1; k_2) = {\sum_{n_2}}' J(n_1, n_2) e^{-ik_2\phi_2 n_2}. \tag{10}$$

It can be shown that only a few of the one-dimensional Hamiltonians in Eq. (9) have eigenstates that may contribute to the absorption spectrum.[1] More specifically, the $k_2 = 0$ band gives contributions that are polarized in the cylinder axis direction, while the degenerate $k_2 = \pm 1$ bands give contributions that are polarized perpendicular to the cylinder axis; all other bands are dark. Moreover, even within these three special bands only very few states have significant oscillator strength. In particular, for the $k_2 = 0$ band there is one superradiant transition that dominates the optical response, while for the $k_2 = \pm 1$ band there will in general be a few, energetically close states that will contain a reasonable oscillator strength.[1,29] The absorption spectrum is thus expected to be dominated by one peak polarized in the cylinder axis direction, and one peak (or for very narrow linewidths, up to three peaks close in energy[29]) polarized perpendicular to the cylinder axis. This can be confirmed explicitly when one assumes periodic boundary conditions in the direction of the cylinder axis (appropriate for long cylinders), where we find that only the above two peaks occur in the absorption spectrum.[1]

When we account for disorder, the states will no longer be extended over the entire circumference of the cylinder, but they will localize over a smaller region instead. As a result of this breaking of the cylindrical symmetry, it is expected that the selection rules obtained for the homogeneous cylinder will no longer exactly hold. The extent to which these selection rules are violated is detailed in Secs. III and IV. Such deviations should be visible in a polarization dependent absorption spectrum taken in an oriented sample.[6,23,38,39]

III. CHARACTERIZING EXCITON STATES IN DISORDERED CYLINDERS

As mentioned in Sec. II C, the presence of disorder induces localization of the exciton states. To quantify this behavior, a number of different measures exist,[27,33,35,40–44] each giving an estimate of the number of molecules that coherently participate in a given exciton state. We will consider here the autocorrelation function of the exciton wave function,[35,42–44] which is particularly useful to probe not only the size but also the directionality of the localization on the cylinder surface. For a given exciton state, it is defined as

$$C_q(\vec{n}) = \sum_{\vec{m}} \left| \varphi_{q\vec{m}} \varphi^*_{q(\vec{n}+\vec{m})} \right|, \tag{11}$$

where the components of $\vec{n}$ and $\vec{m}$ should be taken consistent with the type of boundary conditions we take. For open boundary conditions in the cylinder axis direction, we have: $n_1 = (-N_1 + 1, ..., N_1 - 1)$, $n_2 = (0, 1, ..., N_2 - 1)$, $m_1 = (1, ..., N_1 - n_1)$ for $n_1 \geq 0$, $m_1 = (1 - n_1, ..., N_1)$ when $n_1 < 0$, and $m_2 = (1, ..., N_2)$.

The autocorrelation function measures the correlation between the wave function at positions separated by the vector $\vec{n}$; because of normalization of the wave functions it obeys $C_q(\vec{0}) = 1$, while, generally, it will fall off for growing $|\vec{n}|$. For the cylindrical structures, $C_q(\vec{n})$ has a two-dimensional argument, and as a result we can obtain information on how an exciton state is extended on the cylindrical surface. From the autocorrelation function one can define a measure for the number of molecules that coherently participate in a given exciton state, which we will denote by N_{coh}. For the cylindrical aggregates, N_{coh} has previously been defined in Ref. 35 as the total number of molecules $\vec{n}$ with $C_q(\vec{n}) > 1/e$. Here we will not use that definition of N_{coh}, but rather define it as proposed in Ref. 44: $N_{\text{coh}} \equiv \sum_{\vec{n}} C_q(\vec{n})$. Clearly, states that are localized on a single molecule (strong disorder) give $N_{\text{coh}} = 1$. For states that are completely delocalized (no disorder) we find using periodic boundary conditions along the cylinder axis that $N_{\text{coh}} = N$. Comparing the above two different definitions of N_{coh}, it is clear that the latter definition is less sensitive to fluctuations in the correlation function (due to the summation). It should be noted that in the same way one can also define a measure for the localization of exciton states in certain preferential directions, as will be detailed in Sec. IV.

The extent to which the optical selection rules are violated is expected to be related to the amount of localization in the ring direction. If a state is still extended over (close to) the entire circumference of the cylinder, one expects the selection rules to be (approximately) obeyed. On the other hand, if a state is localized on a small part of the circumference of the cylinder, large deviations from the selection rules are expected.

To quantify the violation of selection rules for a given exciton state q, we consider the transition dipole moment vector corresponding to it, which is given by

$$\vec{\mu}_q = \sum_{\vec{n}} \varphi_{q\vec{n}} \vec{\mu}_{\vec{n}}. \tag{12}$$

We use the angle β_q between the transition dipole moment vector of state q and the cylinder axis $\hat{z}$ as a measure of the extent to which the selection rules are violated,

$$\beta_q = \arccos\left(\frac{|\vec{\mu}_q \cdot \hat{z}|}{|\vec{\mu}_q|} \right). \tag{13}$$

For a homogeneous cylinder, all states with a nonzero oscillator strength will have either $\beta_q = 0^\circ$ for the states polarized in the cylinder axis direction ($k_2 = 0$), or $\beta_q = 90^\circ$ for the states polarized perpendicular to the cylinder axis ($k_2 = \pm 1$). Deviations from the selection rules imply deviations of β_q from these two values. In the limit of extremely large disorder (compared to the intermolecular interactions), we expect to have strongly localized exciton states that resemble the molecular excited states, which have a transition dipole moment with a fixed angle $\beta_q \approx \beta_{\vec{n}} = \beta$. As a result, for large disorder values, the distribution of exciton orientation angles β_q should tend to a delta function centered around β.

It should be noted that we will not be concerned with the distribution of β_q itself, but rather focus on the closely related angle resolved oscillator strength, which we define as

$$F(\eta) = \sum_q |\vec{\mu}_q|^2 \, \delta(\eta - \beta_q). \tag{14}$$

For given angle η, $F(\eta)$ simply sums the oscillator strengths of all exciton states that satisfy $\beta_q = \eta$. In this way, the states which are optically dominant will also play the most important role when characterizing the extent to which selection rules are violated in disordered cylinders.

IV. NUMERICAL RESULTS

The cylindrical aggregates of choice that we apply our theory to are C8S3 aggregates. As has been shown in Refs. 6, 7 and 23, these molecules can form double-walled cylindrical structures where the two walls are weakly coupled. Depending on the details of the synthesis, different radii for the walls can be obtained. In particular, for the Direct Route (DR) synthesis, the walls have radii of roughly 5.4 and 7.8 nm, respectively,[6] while for the Alcoholic Route (AR), the radii are reduced to approximately 3.2 and 6.5 nm.[45] As a result, this type of cylindrical structure naturally shows a large variation in radius, which as we will show leads to large differences in localization behavior and optical properties. While the precise structural parameters for the different walls and synthesis routes are not identical, they presumably are close, and in our simulations we do not vary any of these structural parameters in order to isolate the radius dependence. In particular, we choose the DR inner wall parameters from Ref. 6; that is, we have a bricklayer lattice with lattice constants $a = 2.0$ nm and $d = 0.4$ nm, and a lattice shift of $s = 0.488$ nm. We assume a single-molecule transition dipole moment of $\mu = 11.4$ Debye and use extended dipole–dipole interactions with a charge separation distance of $l = 0.7$ nm.[6] We use a rolling angle of $\theta = 50.7^\circ$ ($\beta = \theta$, $\alpha = 0^\circ$), which is slightly larger than the value used in Ref. 6. The advantage is that our value of θ yields a chiral vector that is rather commensurate with the lattice structure (i.e., it intersects with

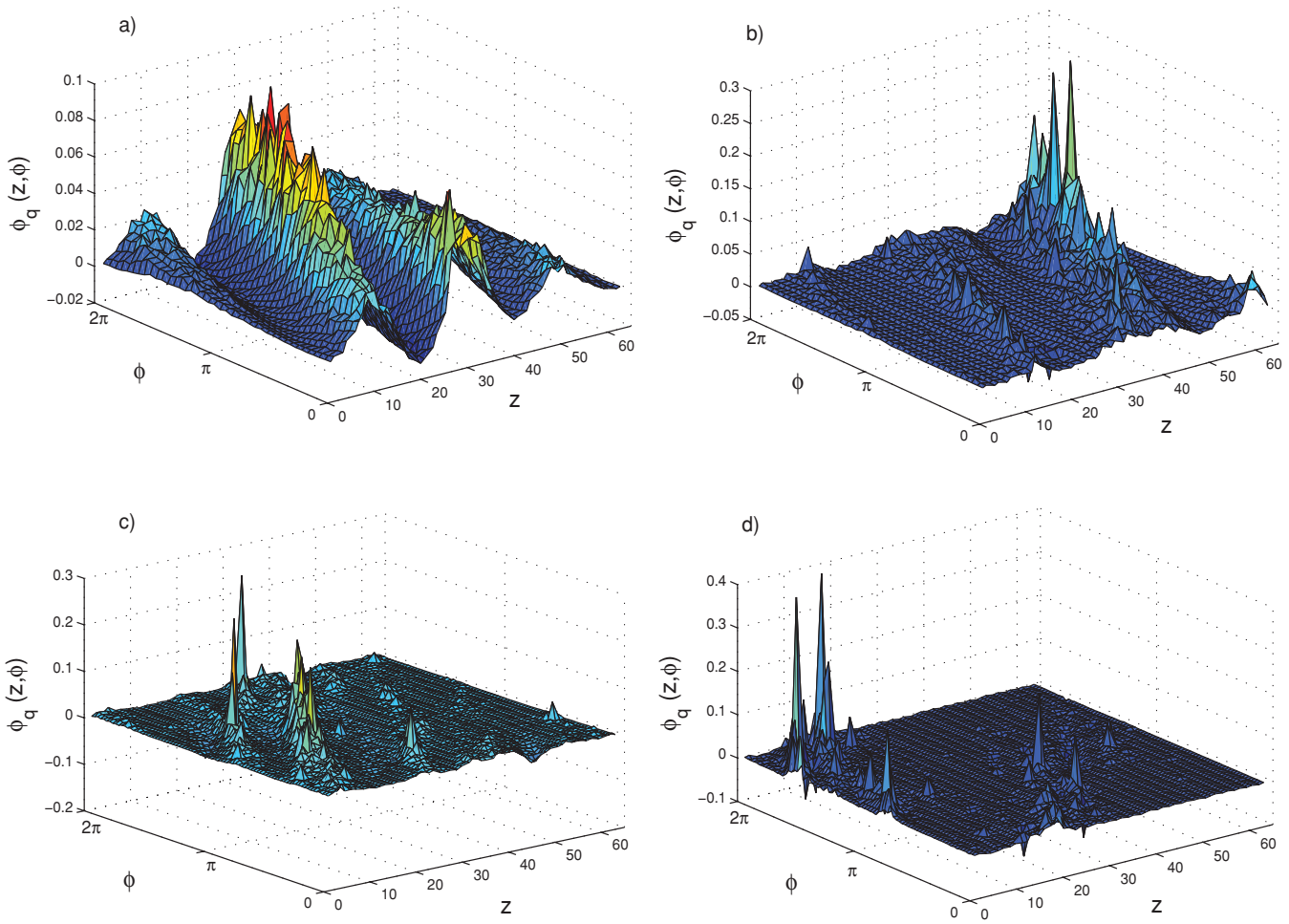

FIG. 2. Exciton wave functions for the state with highest oscillator strength for different disorder magnitudes and radii in a typical realization. [(a) and (b)] $R = 4$ nm, $\sigma = 200$ and 650 cm^{-1}, respectively. [(c) and (d)] $R = 8$ nm, $\sigma = 650$ and 1000 cm^{-1}, respectively. The cylinders have the same length of 63.4 nm; this corresponds to cylinders consisting of $N_1 = 50$ rings with total number of monomers equal to $N = 2000$ ($R = 4$ nm) or $N = 4000$ ($R = 8$ nm). The coordinate z measures the position in the axis direction, while ϕ is the azimuthal angle, measured relative to a line parallel to the cylinder axis.

many lattice points), which facilitates a study of radius dependence and also simplifies the visualization of the wave functions. In our simulations, the cylinders have a length of about 63 nm, which is sufficiently long to eliminate finite size effects for all but the lowest disorder values. One should note that our results are generic and do not depend on the exact choice of the various parameters.

A. Localization of optically dominant states

Before addressing the disorder averaged localization behavior, we first consider a typical disorder realization. In Fig. 2 typical wave functions of the optically most active state are shown for different disorder strengths and for cylinders with radius $R = 4$ nm (corresponding approximately to the inner wall of an Alcoholic Route C8S3 aggregate) and $R = 8$ nm (corresponding approximately to the outer wall of a Direct Route C8S3 aggregate). The wave functions are plotted as a function of the coordinates z and ϕ. Here, z is simply the distance in the cylinder axis direction, while ϕ measures the rotation with respect to some reference line parallel to the cylinder axis (i.e., not relative to the helix in Fig. 1). In other words, $\phi =$ constant is a vertical line on the cylinder surface, and ϕ ranges over an interval of length 2π, which corresponds to one circumference.

Comparison of Figs. 2(a) with 2(b) and 2(c) with 2(d) clearly shows that increasing the disorder while keeping the radius fixed leads to stronger localization, as one expects. It is worthwhile to note that for the weak disorder case, Fig. 2(a), the wave function is rather delocalized. It wraps around the entire cylinder, with coefficients $\varphi_{q\bar{n}}$ that have the same sign practically everywhere, leading to in-phase absorption for all molecules and showing that the state in Fig. 2(a) is indeed a super-radiant state.

Furthermore, several interesting features of the optically dominant state follow from Fig. 2. First, all wave functions have a helical character. This behavior results from the tendency of exciton states to extend in the direction of the strongest interactions. Second, as we anticipated in Sec. II C, fixing the disorder value while increasing the radius will also lead to stronger localization relative to the cylinder circumference in the ring direction. Specifically, while the absolute exciton localization length should be quite similar, the localization length with respect to the cylinder circumference decreases. This can be observed by comparing Figs. 2(b) and 2(c). Finally, an interesting

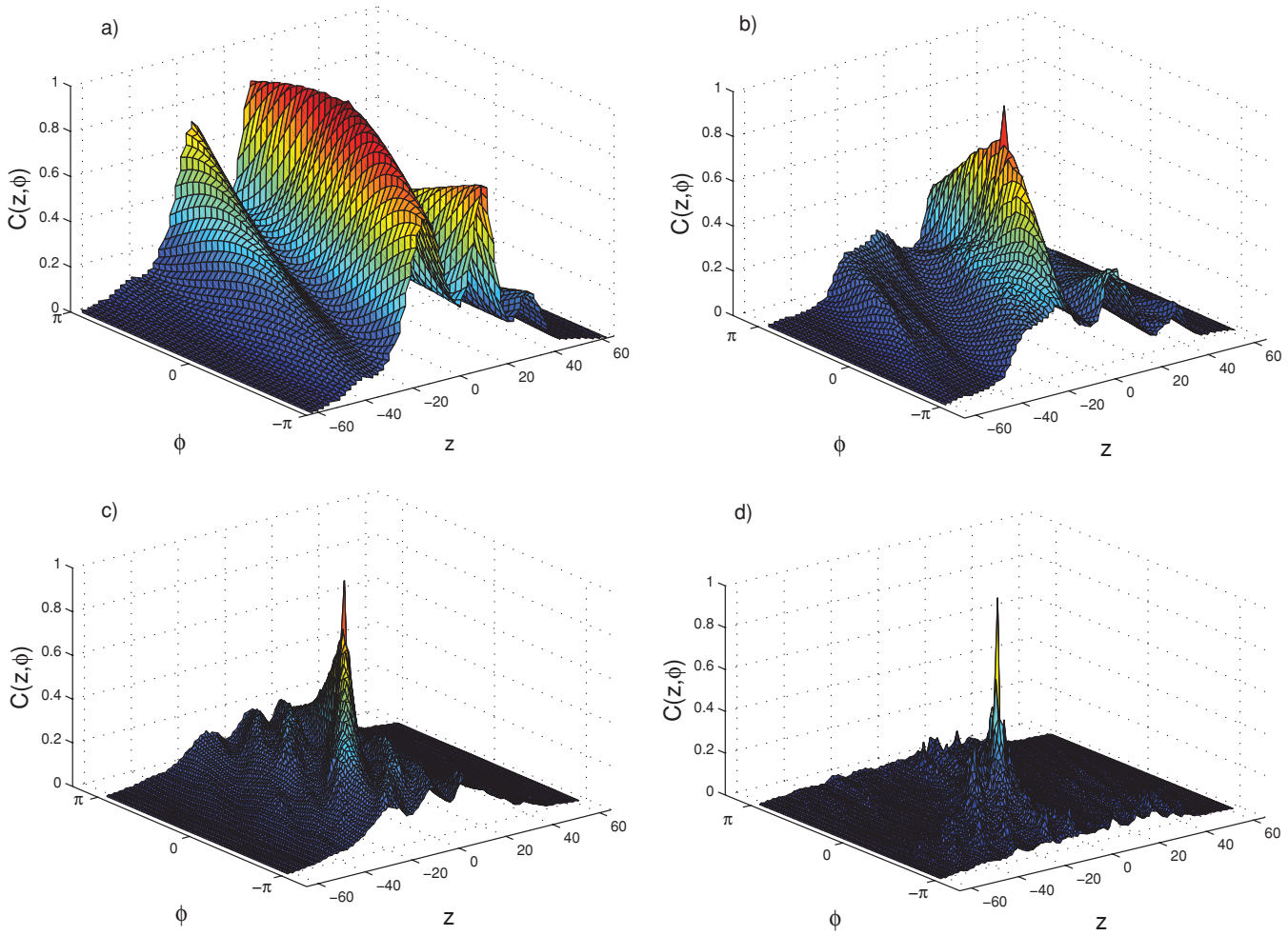

FIG. 3. Autocorrelation functions for the state with highest oscillator strength for different disorder magnitudes and radii in a typical realization. The disorder realization and the parameters are the same as in Fig. 2. Contrary to the irregular structure of the wave functions, the autocorrelation functions are rather smooth, which makes it the preferable quantity to extract the localization lengths.

observation on the wave functions shown in Figs. 2(b)–2(d) is the fact that there tend to be multiple regions where the wave function has appreciable values. This is in contrast to the one-dimensional case,[46] but is fully consistent with the multifractal nature of the excited states that has been observed previously in two-dimensional (and higher-dimensional) lattices.[47,48]

In Fig. 3 we present the autocorrelation functions corresponding to the wave functions of Fig. 2. As in the case of the wave functions, the autocorrelation function is also plotted as a function of z and ϕ. The autocorrelation functions clearly corroborate the features already seen for the wave functions; that is, the helical orientation and the increased amount of (relative) localization upon both increasing disorder strength and increasing radius. However, the smoother structure of the autocorrelation function compared to the wave function [resulting from the summation over $\vec{m}$ in Eq. (11)] makes it the preferred quantity to extract the (relative) localization lengths.

So far we have discussed the qualitative features of the exciton state with the highest oscillator strength. To make the above observations more quantitative, we will calculate the exciton localization length in the direction of the strongest interactions, i.e., along the helical orientation seen in Fig. 3, relative to the tube's circumference. This quantity, here after abbreviated as relative localization length, will be denoted by Λ and for a given exciton state q is expressed as

$$\Lambda \equiv \frac{L_\phi}{2\pi R}. \tag{15}$$

Here $L_\phi = \sum_z' C_q^{\max}(z,\phi)$, with $C_q^{\max}(z,\phi)$ denoting the maximum value of the autocorrelation function at position z and the restricted summation includes only values of $C_q^{\max}(z,\phi)$ above a threshold value C_0. Thus, L_ϕ is a measure for the extent of the excitonic wave functions in the helical direction. It should be noted that we have introduced a threshold value C_0 in the definition of L_ϕ, thus neglecting contributions from small values of $C_q^{\max}(z,\phi)$. The reason for this is that for these small values (which occur at large values of $|z|$), the autocorrelation function is no longer oriented in the helical direction due to the fractal nature of the wave functions. Rather, these small values $C_q^{\max}(z,\phi)$ appear to be randomly distributed along the different rings. Therefore, these values have not been included in the calculation of L_ϕ. For the threshold value we always take $C_0 = 0.3$, which is slightly lower than the value $1/e$ used in Ref. 35.

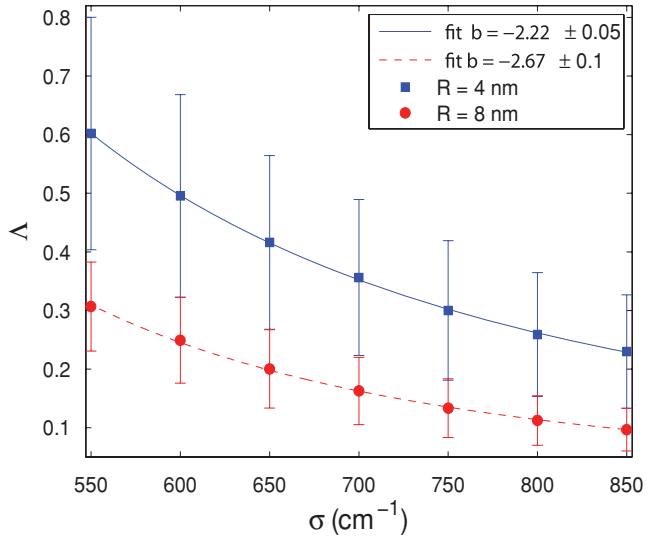

FIG. 4. Mean and standard deviations (denoted by error bars) of the relative localization lengths Λ of the optically dominant states. For each disorder value, 75 realizations were taken into account. For each realization only states that contain at least 10% of the maximum oscillator strength of that realization are accounted for. The data points are fitted by a power law with exponent $b \approx -2.2$ for $R = 4$ nm and $b \approx -2.7$ for $R = 8$ nm. For a particular disorder value, the average relative localization is approximately a factor of 2 bigger for the cylinder with small radius ($R = 4$ nm), which implies that the absolute localization length is the same for both cylinders.

As we are only interested in the optically relevant states, for each disorder realization, we consider only those states that contain at least 10% of the maximum oscillator strength of that realization. For each of those states, and for a number of disorder realizations, the localization measure Λ was obtained, resulting in a distribution for Λ. Figure 4 presents the means $\langle\Lambda\rangle$ and standard deviations (denoted as error bars) of this distribution for various values of the disorder strength and cylinders with radius $R = 4$ nm and $R = 8$ nm. It clearly shows that, for both radii, an increase of the disorder leads to a decrease of $\langle\Lambda\rangle$. Furthermore, for a given value of σ, $\langle\Lambda\rangle$ for the cylinder with radius $R = 4$ nm is approximately twice as large as for the cylinder with radius $R = 8$ nm (this ratio increases somewhat with increasing disorder strength). This is not surprising, because for a particular value of σ the absolute localization length L_ϕ is roughly the same for both radii, as is expected from the fact that the underlying two-dimensional lattice structure is identical. It should be noted that the fluctuations in Λ are of the same order of magnitude as its mean value, which has also been found previously in one-dimensional lattices.[49]

An interesting aspect of Fig. 4 is the scaling of the localization length with disorder. Previous studies addressing localization behavior in aggregate systems,[33,41,46,50] have established both by analytical arguments and numerical simulations that the scaling relation is well described by a power law dependence. We found that the data in Fig. 4 may also be accurately fitted to a power law, $\langle\Lambda\rangle = a\sigma^b$, with corresponding exponents for both cylinders that are large ($b \approx -2.2$ for $R = 4$ nm and $b \approx -2.7$ for $R = 8$ nm) in comparison to the well-known scaling behavior in one dimension, where the exponent is approximately given by $b \approx -2/3$.[33,41] In Refs. 46 and 50, it was shown that the exponent can be obtained by equating the typical energy spacing between the lowest energy states on a localization segment to the disorder induced scattering rate between these states. Unfortunately, as a result of the two-dimensional nature of the cylindrical surface and the long-range dipolar interactions that are present, both the energy spacing and the disorder induced scattering rate scale with the localization size in a very similar way, making it impossible to use the simple arguments of Refs. 46 and 50 to analytically predict the disorder scaling of the localization length seen in Fig. 4. Also, the range of disorder values that can be studied numerically is limited either due to the system size (in case of small disorder) or due to the number of necessary realizations (for large disorder values) so that it is not possible to examine how the power law behavior holds in these limiting cases. A more detailed investigation of the scaling behavior in situations where the scattering rate scales in a similar way with the localization size is subject to ongoing research.

B. Breaking of the selection rules

In the previous section we established the localization behavior of exciton states for cylinders with different radii. Now we will address the consequences of localization for the optical selection rules. As mentioned in Sec. III, it is straightforward to calculate to what extent selection rules are violated for various choices of the disorder. For each realization, we simply calculate all eigenstates, their transition dipoles, and then evaluate the angular distribution function $F(\eta)$ for the oscillator strength, defined in Eq. (14). The results are shown in Fig. 5. Obviously, these results are mainly determined by the optically dominant states, as the contribution of states with no or very little oscillator strength is negligible.

Figure 5(a) has been obtained for the cylinder with radius $R = 4$ nm, with a (small) disorder value $\sigma = 200$ cm^{-1} (smaller than occurs in experiment[6]). As expected for small disorder values, the states with an appreciable oscillator strength still have dipoles oriented close to the cylinder axis or perpendicular to it (corresponding to transitions to the $k_2 = 0$ states and the $k_2 = \pm 1$ states, respectively). Indeed, this is clearly seen in Fig. 5(a). Increasing the disorder to a more reasonable value[6] of $\sigma = 650$ cm^{-1} and keeping the radius fixed, we see clearly from Fig. 5(b) an increase of the oscillator strength in orientations which are not allowed in the homogeneous case, and thus an increase in the extent to which the selection rules are violated. This is in agreement with Fig. 4, which showed that the relative localization length decreased, and thus deviations from the selection rules are expected to become larger, upon increasing the disorder strength.

Increasing the radius of the cylinder to $R = 8$ nm while keeping the disorder value fixed at $\sigma = 650$ cm^{-1} leads to the oscillator strength distribution of Fig. 5(c). It is clearly seen here that the selection rules are broken to a much larger extent than for the cylinder with smaller radius $R = 4$ nm, as shown in Fig. 5(b). This finding is also in agreement with the results of Fig. 4, where it was shown that upon increasing the radius

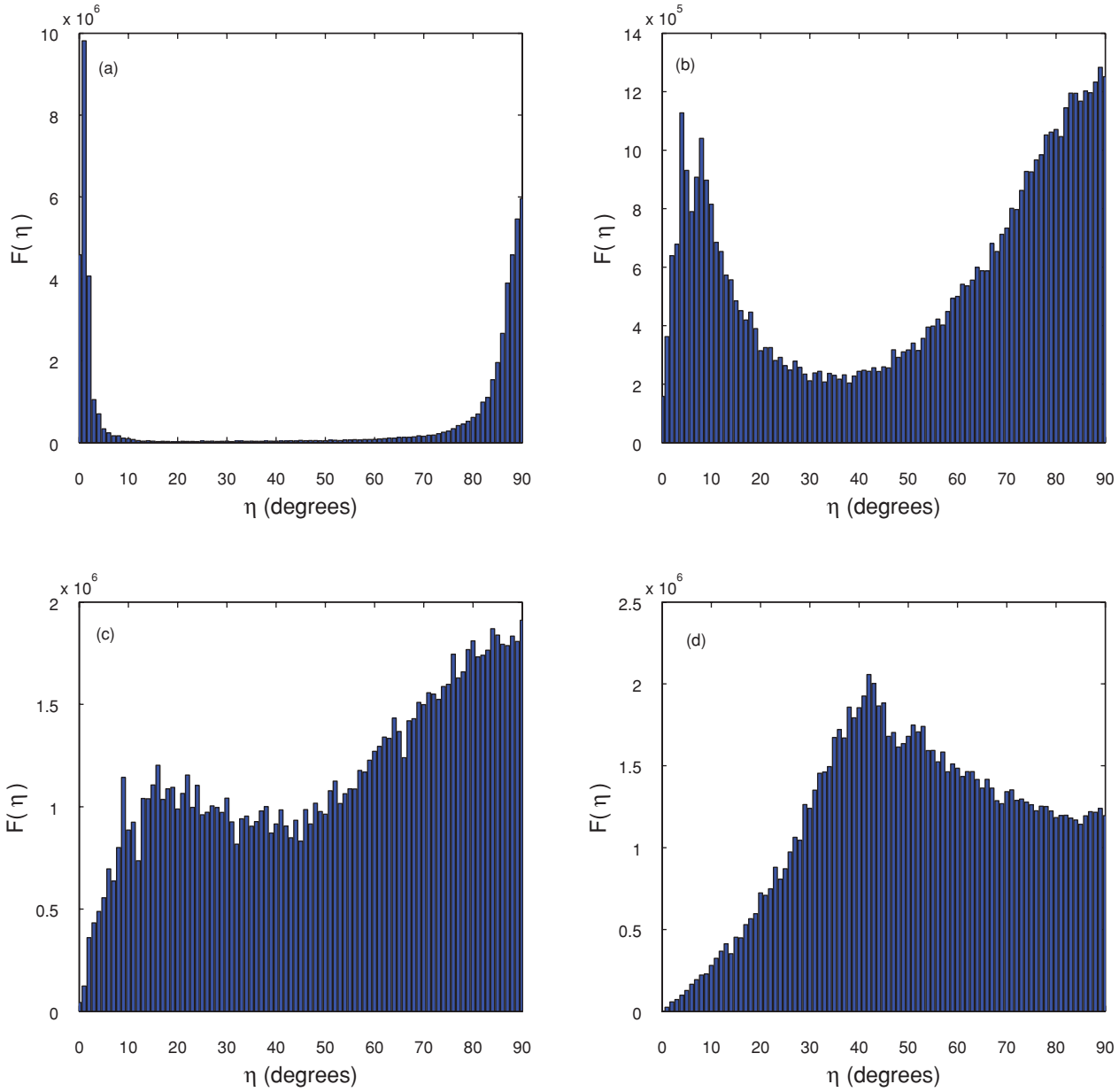

FIG. 5. Angle resolved oscillator strength distributions for different disorder values and radii. [(a) and (b)] $R = 4$ nm, $\sigma = 200$ and 650 cm^{-1}, respectively. [(c) and (d)] $R = 8$ nm, $\sigma = 650$ and 1000 cm^{-1}, respectively. For each panel, 200 realizations of disorder were taken into account. Deviations from the ideal selection rules that exist for a homogeneous cylinder become more pronounced for increasing disorder and larger radius. The fluctuations still apparent in the distributions are of statistical nature, and will thus disappear with increasing number of realizations.

at a constant disorder strength, the relative localization length becomes smaller, and thus deviations from the selection rules become more pronounced. Eventually, upon further decrease of the relative localization length [Fig. 5(d)], convergence sets in toward a distribution centered around the monomer dipole orientation β (which is the rolling angle, $\beta = \theta = 50.7^\circ$), where in the extreme case of very large disorder all oscillator strength should be collected.

Besides the above observations, we note that the oscillator strength distributions in Fig. 5 show an asymmetry between small and large angles. There is almost no oscillator strength at an orientation angle $\eta = 0^\circ$, while the weight at larger angles η is enhanced considerably. The reason for this is purely geometrical; there exist only very few orientations of $\vec{\mu}_q$ such that $\eta \approx 0^\circ$. More specifically, the phase space volume of possible orientations grows proportional to $\sin(\eta)$, simply because the area of the part of the sphere with an inclination angle between η and $\eta + d\eta$ is given by $A(\eta) = 2\pi \sin \eta d\eta$. This explains the skewing of the oscillator strength distributions in Fig. 5 toward larger angles.

We have so far qualitatively discussed the role of localization for the violation of the optical selection rules and established that a decrease of the localization relative to the tubes circumference leads to a larger amount of violation of the optical selection rules. To further support our findings

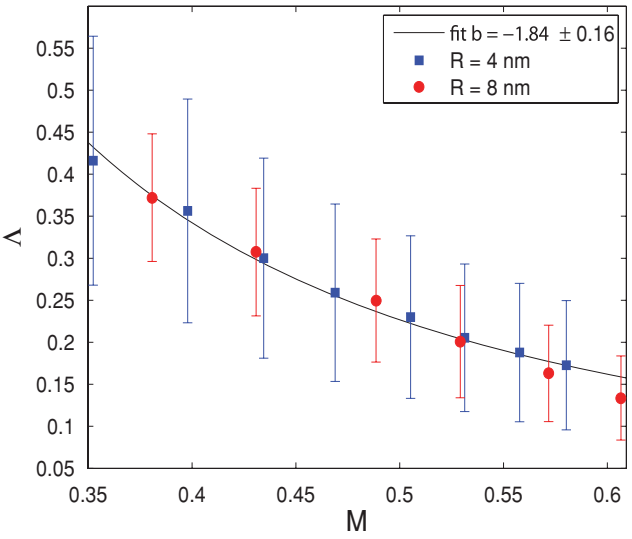

FIG. 6. Mean and standard deviations (denoted by error bars) of the relative localization lengths Λ vs the measure M for cylinders with different radii and various disorder values. For $R = 4$ nm: $\sigma = 650$ –1000 cm^{-1} in steps of 50 cm^{-1}; for $R = 8$ nm: $\sigma = 500$–750 cm^{-1} in steps of 50 cm^{-1}. For each data point, 75 realizations of disorder were taken into account. The data points are fitted to a power law with exponent $b \approx -1.8$. This figure shows that different cylinders with the same relative localization $\langle\Lambda\rangle$ also have the same amount of violation of optical selection rules.

that the relative localization length Λ is the parameter that governs the breakdown of the selection rules, we consider the following measure, denoted by M, to quantify the extent to which the selection rules are broken:

$$M = \sum_{\eta=20^\circ}^{70^\circ} F(\eta) / \sum_{\eta=0^\circ}^{90^\circ} F(\eta). \tag{16}$$

In this way, we have a measure for the violation of selection rules that equals zero for the homogeneous cylinder ($\sigma = 0$ cm^{-1}), increases with increasing disorder, and tends to unity in the limit of extremely large disorder (if $20^\circ \leq \beta \leq 70^\circ$). Obviously, the chosen range of $20^\circ \leq \eta \leq 70^\circ$ is rather arbitrary, and different intervals for η may be considered to define the measure M. The consequences of this are discussed at the end of this section.

In Fig. 6 we show for various values of the disorder and two cylinders with distinct radii the measure M and the corresponding mean relative localization length $\langle\Lambda\rangle$ (error bars denoting the standard deviations). Clearly, for both cylinders a decrease of $\langle\Lambda\rangle$ leads to an increase of M as we have anticipated before. Most interestingly, cylinders with different radii that have roughly the same relative localization lengths $\langle\Lambda\rangle$ (and thus different disorder strengths) also have the same measure M. This is expressed by the fact that all data points (of both cylinders) follow the same curve in Fig. 6. This curve may be fitted to a power law $\langle\Lambda\rangle = aM^b$ with exponent $b \approx -1.8$. The range of measures M for which the data points for different radii follow the same curve is expected to break down at large values of the disorder, i.e., at large values of M. A signature of this in Fig. 6 seems to be that for the larger values of M, the data points for the cylinder with radius $R = 8$ nm have a tendency to lie below the curve. The reason for this trend becomes obvious if one considers the limit of very large disorder. In this case, all states are localized on a single molecule and the transition dipoles are simply given by β. This means that both cylinders have the same measure $M = 1$ although their relative localization lengths Λ differ by a factor of 2.

As mentioned above, the definition for the measure M [Eq. (16)] is somewhat arbitrary in the way the range of η is chosen. We have compared our findings with other intervals for η, ranging from $15^\circ \leq \eta \leq 75^\circ$ up to $30^\circ \leq \eta \leq 60^\circ$. It was found that although the exact value of the exponent of the power law fit does depend on the chosen interval, our main conclusion that the fitted curve is independent of the radius of the cylinder holds for all definitions of M.

C. Absorption spectra

To connect more closely to experiment, we have also calculated the absorption spectra for disordered cylindrical aggregates. In Fig. 7, we show the various absorption spectra $A_0(\omega)$, $A_{||}(\omega)$, and $A_\perp(\omega)$ for cylindrical aggregates of two different radii: $R = 4$ nm and $R = 8$ nm, both with the molecular arrangement used throughout this paper and a disorder strength of $\sigma = 650$ cm^{-1}, which is quite typical of the experimentally found value for C8S3 aggregates.[6] The difference in structure in the absorption spectra is clear. For the cylinder with a small radius, a clear two-peak structure can still be observed in the isotropic absorption spectrum [Fig. 7(a)]: a low-energy peak corresponding to transitions that are approximately polarized in the axis direction, and a higher energy peak corresponding to transitions that are approximately polarized perpendicular to the cylinder axis. This is corroborated by the polarization dependent absorption spectra shown in Fig. 7(c) and also in agreement with the results obtained for the angle resolved oscillator strength distribution [Fig. 5(b)]. In contrast, for a system with the same disorder value but a larger radius ($R = 8$ nm), the selection rules are broken to a much larger extent. The peaks polarized parallel and perpendicular to the cylinder axis overlap to a large degree [Fig. 7(d)] and the isotropic spectrum shows hardly any structure [Fig. 7(b)]. The reason is that the absorption comes from a large bulk of states with widely varying polarizations [Fig. 5(c)], instead of two distinct groups of states with polarizations either near 0° or 90°.

Thus, the general conclusion is that, keeping the disorder strength fixed, the absorption spectrum loses structure upon increasing the cylinder radius, which is a consequence of an enhanced breaking of the optical selection rules in the wider cylinder.

The above conclusion is in qualitative agreement with the experimental findings reported in Ref. 32. There, the absorption spectra of the inner and outer wall cylinders of C8S3 aggregates were separated through preferentially perturbing the molecules within the outer wall cylinder by means of chemical oxidation, effectively switching off the optical response of the outer wall at a higher rate. The resulting inner wall spectrum exhibits a rich spectral structure with multiple (at least four) well separated transitions, which can likely be

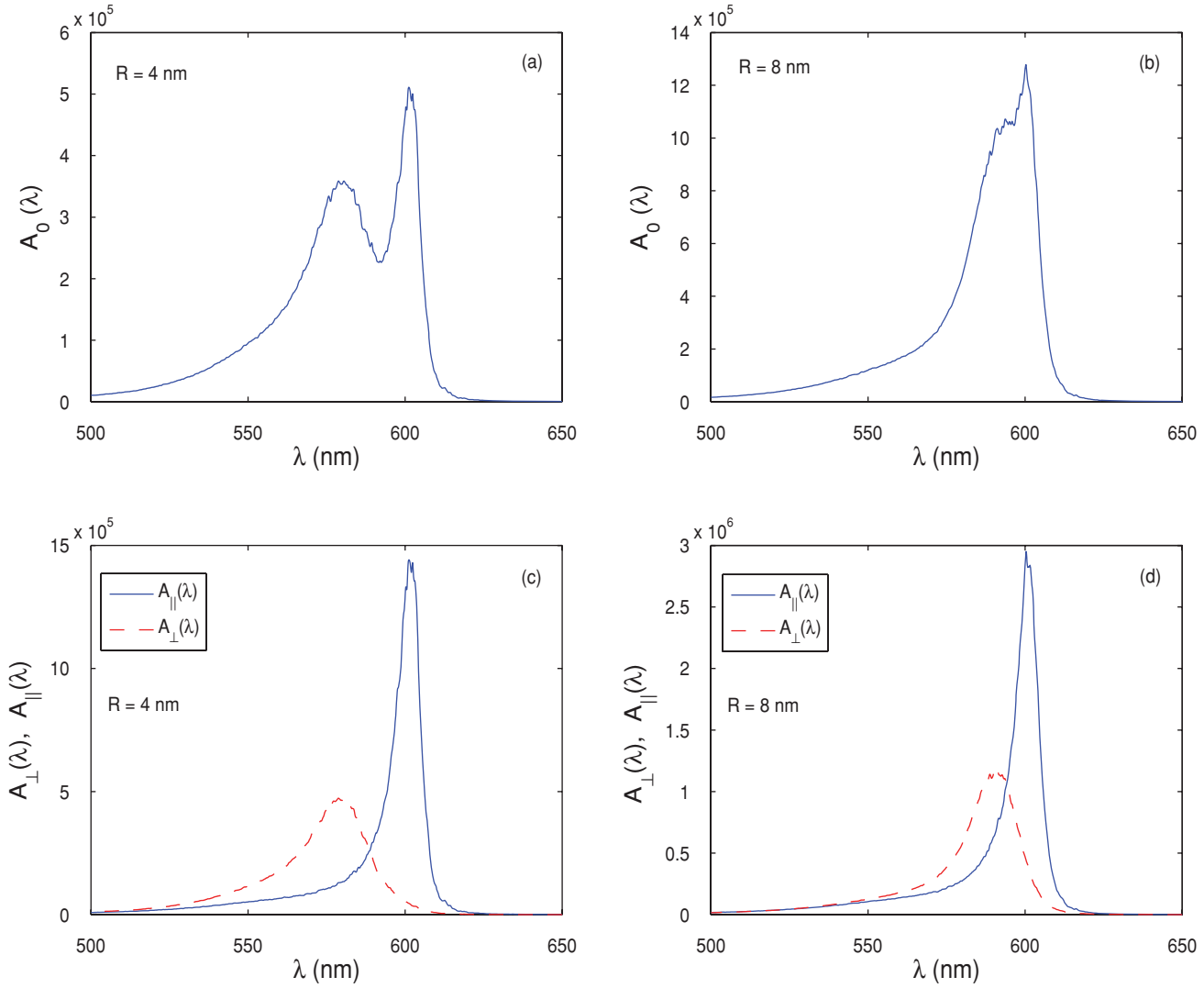

FIG. 7. Absorption spectra for two cylinders with a distinct radius and a fixed disorder $\sigma = 650\ \mathrm{cm}^{-1}$. [(a) and (b)]: Isotropic absorption spectra $A_0(\omega)$ for radii $R = 4$ nm and $R = 8$ nm, respectively. [(c) and (d)]: Corresponding polarization dependent spectra $A_{||}(\omega)$ and $A_{\perp}(\omega)$ for the two radii.

interpreted as two Davydov-split doublets. The low energy doublet in the absorption spectrum of the inner wall shows two well-separated peaks, in contrast to the outer wall absorption which hardly shows any spectral structure (likely only two transitions close in energy with one appearing as a shoulder of the other).

V. SUMMARY

The unavoidable presence of disorder in cylindrical molecular aggregates will lead to localization of the collective electronic excited states and a breakdown of the optical selection rules that exist for a perfect cylindrical symmetry, and which are often used to explain the experimental absorption spectra. Using numerical simulations we have shown that localization indeed occurs, leading to deviations from the homogeneous situation, but depending on the disorder magnitude and the radius of the cylinder, the selection rules may still apply to a large extent. The relevant quantity to determine this is the relative localization length Λ, i.e., the exciton localization length relative to the total cylinder circumference. As a result, both increasing the disorder (and thus decreasing the localization length) and increasing the radius (and thus the circumference) will lead to stronger deviations from the homogeneous selection rules. We have shown and quantified this by analyzing the distribution of polarizations of the exciton states with nonzero oscillator strength, and using this distribution to define a measure M to quantify the extent to which the selection rules are broken. We have found that both an increase of the disorder strength and an increase of the cylinder radius result in larger values of M. Most importantly, we have shown that plotting $\langle\Lambda\rangle$ against M, a curve is found that does not depend on the radius of the cylinder. This proves that, indeed, the relative localization length governs the breaking of the selection rules.

The structure of the wave functions and their autocorrelation functions obviously show localization as well. In particular, both an increasing disorder strength and an increasing radius will show stronger localization relative to the circumference. We find that both the wave functions and the autocorrelation functions are helically oriented, in the direction of the strongest interactions. An interesting observation is that the

exciton wave functions tend to have multiple regions where the amplitude is nonzero; this is consistent with the multifractal nature of the two-dimensional exciton states as suggested by Schreiber and co-workers.[47,48]

Finally, the localization and the resulting breaking of the selection rules has direct consequences for the (polarization dependent) absorption spectra. Quite generally, keeping the disorder strength fixed, the absorption spectrum loses structure upon increasing the cylinder radius, which is a consequence of an enhanced breaking of the optical selection rules in the wider cylinder. The separate peaks in the smaller-radii cylinders have polarization directions either mostly parallel or mostly perpendicular to the cylinder axis. For the structureless spectra of the larger-radii cylinders this polarization information is lost, because the underlying exciton states have a wide range of polarization orientations. These findings are in qualitative agreement with recent experiments.[32]

ACKNOWLEDGMENTS

We thank Professors D. A. Vanden Bout and J. P. Rabe and Dr. D. M. Eisele for stimulating discussions and for sharing experimental results with us prior to publication.

[1]C. Didraga, J. A. Klugkist, and J. Knoester, J. Phys. Chem. B **106**, 11474 (2002).
[2]A. Pawlik, S. Kirstein, U. DeRossi, and S. Dähne, J. Phys. Chem. B **101**, 5646 (1997).
[3]H. von Berlepsch, A. Ouart, M. Regenbrecht, S. Akari, U. Keiderling, H. Schnablegger, S. Dähne, and S. Kirstein, Langmuir **16**, 5908 (2000).
[4]A. Pugžlys, R. Augulis, P. H. M. van Loosdrecht, C. Didraga, V. Malyshev, and J. Knoester, J. Phys. Chem. B **110**, 20268 (2006).
[5]H. von Berlepsch, C. Böttcher, A. Ouart, C. Burger, S. Dähne, and S. Kirstein, J. Phys. Chem. B **104**, 5255 (2000).
[6]C. Didraga, A. Pugžlys, P. R. Hania, H. von Berlepsch, K. Duppen, and J. Knoester, J. Phys. Chem. B **108**, 14976 (2004).
[7]D. M. Eisele, J. Knoester, S. Kirstein, J. P. Rabe, and D. A. Vanden Bout, Nat. Nanotech. **4**, 658 (2009).
[8]O. Ohno, Y. Kaizu, and H. Kobayashi, J. Chem. Phys. **99**, 4128 (1993).
[9]R. F. Pasternack, K. F. Schaefer, and P. Hambright, Inorg. Chem. **33**, 2062 (1993).
[10]S. C. M. Gandini, E. L. Gelamo, R. Itri, and M. Tabak, Biophys. J. **85**, 1259 (2003).
[11]Z. Wang, C. J. Medforth, and J. A. Shelnutt, J. Am. Chem. Soc. **126**, 15954 (2004).
[12]S. M. Vlaming, R. Augulis, M. C. A. Stuart, J. Knoester, and P. H. M. van Loosdrecht, J. Phys. Chem. B **113**, 2273 (2009).
[13]H. Tamiaki, M. Amakawa, Y. Shimono, R. Tanikaga, A. R. Holzwarth, and K. Schaffner, Photochem. Photobiol. **63**, 92 (1996).
[14]V. I. Prokhorenko, A. R. Holzwarth, M. G. Müller, K. Schaffner, T. Miyatake, and H. Tamiaki, J. Phys. Chem. B **106**, 5761 (2002).
[15]H. van Amerongen, L. Valkunas, and R. van Grondelle, *Photosynthetic Excitons* (World Scientific, Singapore, 2000).
[16]L. A. Staehelin, J. R. Golecki, and G. Drews, Biochim. Biophys. Acta **589**, 30 (1980).
[17]G. T. Oostergetel, M. Reus, A. Gomez Maqueo Chew, D. A. Bryant, E. J. Boekema, and A. R. Holzwarth, FEBS Lett. **581**, 5435 (2007).
[18]T. Renger, V. May, and O. Kühn, Phys. Rep. **343**, 317 (2001).
[19]W. Moffitt, J. Chem. Phys. **25**, 467 (1956).
[20]W. Moffitt, D. D. Fitts, and J. G. Kirkwood, Proc. Natl. Acad. Sci. U.S.A. **43**, 723 (1957).
[21]J. S. Briggs and A. Herzenberg, J. Phys. B: Atom. Molec. Phys. **3**, 1663 (1970); Mol. Phys. **21**, 865 (1971).
[22]J. Knoester and S. Daehne, Int. J. Photoenergy **2006**, 1 (2006).
[23]H. von Berlepsch, S. Kirstein, R. Hania, A. Pugžlys, and C. Böttcher, J. Phys. Chem. B **111**, 1701 (2007).
[24]R. Augulis, A. Pugžlys, and P. H. M. van Loosdrecht, Phys. Status Solidi C **3**, 3400 (2006).
[25]F. Milota, J. Sperling, A. Nemeth, and H. F. Kauffmann, Chem. Phys. **357**, 45 (2009).
[26]A. Nemeth, F. Milota, J. Sperling, D. Abramavicius, S. Mukamel, and H. F. Kauffmann, Chem. Phys. Lett. **469**, 130 (2009).
[27]T. Meier, Y. Zhao, V. Chernyak, and S. Mukamel, J. Chem. Phys. **107**, 3876 (1997).
[28]C. Spitz, J. Knoester, A. Ouart, and S. Daehne, Chem. Phys. **275**, 271 (2002).
[29]C. Didraga and J. Knoester, J. Chem. Phys. **121**, 946 (2004).
[30]J. Adolphs and T. Renger, Biophys. J. **91**, 2778 (2006).
[31]P. W. Anderson, Phys. Rev. **109**, 1492 (1958); E. Abrahams, P. W. Anderson, D. C. Licciardello, and T. V. Ramakrishnan, Phys. Rev. Lett. **42**, 673 (1979).
[32]D. M. Eisele, C. W. Cone, J. P. Rabe, and D. A. Vanden Bout, *private communications*.
[33]H. Fidder, J. Knoester, and D. A. Wiersma, J. Chem. Phys. **95**, 7880 (1991).
[34]V. I. Prokhorenko, D. B. Steensgaard, and A. R. Holzwarth, Biophys. J. **85**, 3173 (2003).
[35]C. Didraga and J. Knoester, J. Chem. Phys. **121**, 10687 (2004).
[36]V. M. Agranovich and M. D. Galanin, in *Electronic Excitation Energy Transfer in Condensed Matter*, edited by V. M. Agranovich and A. A. Maradudin (North-Holland, Amsterdam, 1982).
[37]A. S. Davydov, *Theory of Molecular Excitons* (Plenum, New York 1971).
[38]U. De Rossi, S. Dähne, S. C. J. Meskers, and H. P. J. M. Dekkers, Angew. Chem. **108**, 827 (1996).
[39]M. H. C. Koolhaas, R. N. Frese, G. J. S. Fowler, T. S. Bibby, S. Georgakopoulou, G. van der Zwan, C. N. Hunter, and R. van Grondelle, Biochemistry **37**, 4693 (1998).
[40]D. J. Thouless, Phys. Rep. **13**, 93 (1974).
[41]M. Schreiber and Y. Toyozawa, J. Phys. Soc. Jpn. **51**, 1528 (**1982**); *ibid.* **51**, 1537 (1982).
[42]M. Chachisvilis, O. Kühn, T. Pullerits, and V. Sundström, J. Phys. Chem. B **101**, 7275 (1997).
[43]O. Kühn and V. Sundström, J. Chem. Phys. **107**, 4154 (1997).
[44]F. C. Spano, J. Clark, C. Silva, and R. H. Friend, J. Chem. Phys. **130**, 074904 (2009).
[45]D. M. Eisele, H. von Berlepsch, C. Böttcher, K. J. Stevenson, D. A. Vanden Bout, S. Kirstein, and J. Rabe, J. Am. Chem. Soc. **132**, 2104 (2010).
[46]V. Malyshev and P. Moreno, Phys. Rev. B **51**, 14587 (1995).
[47]M. Schreiber, Phys. Rev. B **31**, 6146 (1985).
[48]M. Schreiber, Physica A **167**, 188 (1990); N. Tit and M. Schreiber, J. Phys.: Condens. Matter **7**, 5549 (1995).
[49]A. V. Malyshev and V. A. Malyshev, Phys. Rev. B **63**, 195111 (2001).
[50]V. A. Malyshev, Opt. Spektrosk. 71, 873 (1991); [Opt. Spectrosc. **71**, 505 (1991)]; J. Lumin. **55**, 225 (1993).